Title:

A novel methodological framework for the assessment of the neural control of the shoulder using high-density surface electromyography.

Authors:
J. Greig Inglis[1], Silvia Rio[1], Hélio V. Cabral[2,3,4], Caterina Cosentino[1], Roberto Pagani[5], Tea Lulic-Kuryllo[6,7], Clark R Dickerson[7], Francesco Negro[1]

Affiliations:
[1]Department of Clinical and Experimental Sciences, Università degli Studi di Brescia, Brescia, Italy
[2]School of Physical Education and Sports, Universidade Federal do Rio de Janeiro, Rio de Janeiro, Brazil
[3]Biomedical Engineering Program (COPPE), Universidade Federal do Rio de Janeiro, Rio de Janeiro, Brazil
[4]Postgraduate Program in Rehabilitation Sciences, Universidade Federal do Rio de Janeiro, Rio de Janeiro, Brazil
[5]Department of Mechanical and Industrial Engineering, Università degli Studi di Brescia, Brescia, Italy
[6]Office of Research, Waterloo Regional Health Network, Kitchener, Canada
[7]Department of Kinesiology and Health Sciences, University of Waterloo, Waterloo, Canada

Conflict of Interest:
The authors report no conflict of interest.

Funding:
This study was funded by the European Research Council Consolidator Grant 'INcEPTION', contract no. 101045605. J Greig Inglis was supported by the Marie Skłodowska-Curie Actions Grant 'MUDecomp', agreement no. 101151712. Silvia Rio was supported by Unione Europea-Next Generation EU, Missione 4, Componente 1, CUP B31I24000510004.

Corresponding author:
Prof. Francesco Negro
Department of Clinical and Experimental Sciences,
Università degli Studi di Brescia
Viale Europa 11, Brescia, 25121, Italy
Email: francesco.negro@unibs.it

ABSTRACT

The complex function of the shoulder relies on the coordinated activation of small and large muscles, including the deltoid, pectoralis major, trapezius, and latissimus dorsi. However, detailed knowledge of their neuromuscular control remains limited. This study aimed to develop a methodological framework to investigate the neural control of the larger superficial shoulder muscles by combining a six-degree-of-freedom load cell attached to a robotic arm with high-density surface electromyograms (HDsEMG). Six healthy participants performed isometric contractions (abduction, adduction, flexion, and extension) at 30% of maximal voluntary contraction with the shoulder positioned at 30° and 65° of lateral abduction. HDsEMGs were recorded from the four muscles and analysed at the global activation, spatial distribution of activation and motor unit levels. Global activation was quantified using averaged normalized root-mean-square (RMS) amplitude and spatial distribution using coefficient of variation of the topographic maps. Moreover, HDsEMGs were decomposed into individual motor unit spike trains using convolutive blind source separation, and motor unit behaviour was characterized by mean discharge rate and spatial distribution of motor unit action potentials (MUAPs). RMS maps revealed action-specific activation within and between muscles, with the upper trapezius active across all tasks, while the anterior, middle, and posterior deltoid, clavicular pectoralis major, and latissimus dorsi were predominantly activated during abduction, flexion, and extension. Motor unit discharge rate also showed task-dependent activity. MUAP spatial distributions further showed distinct motor unit territories within arrays, suggesting region-specific recruitment strategies across actions. In conclusion, this framework demonstrates that individual motor unit activity can be reliably measured non-invasively in the superficial shoulder muscles. The approach provides a methodological basis for novel incorporation of neural control information into biomechanical models of shoulder function.

Keywords: motor unit discharge rate, HDsEMG spatial distribution, neural control, shoulder biomechanics.

1.0 INTRODUCTION

Actions of the humerus require the complex activation of the muscles surrounding the glenohumeral joint to contract and, ultimately, cause the desired action. During these actions, the activation of large muscles such as the *trapezius, pectoralis major, latissimus dorsi,* and *deltoid* must be precisely coordinated with several smaller muscles, in particular the rotator cuff elements, to generate torque across multiple joints and adapt to changes in both task demands and musculoskeletal alterations, while also maintain glenohumeral stability in a delicate balance (Veeger & van der Helm, 2007). According to Hughes and colleagues (1999), the muscles of the glenohumeral joint (hereafter referred to as the shoulder) and their strength are important components of functional capacity. Thus, understanding the neuromuscular behaviour of these muscles is essential for a complete understanding of the activation and function of this muscle group, which can inform the prescription of appropriate training and rehabilitation strategies. Biomechanical modelling of the shoulder relies on simple mechanical analyses of body segments and the internal and external forces acting on the joint to predict shoulder muscle control (Hughes & An, 1997; Chang *et al.*, 2000; Dickerson *et al.*, 2008; Seth *et al.*, 2019). However, to date, there are restrictions on modelling advances in the shoulder, particularly in including neural control of active muscles and, specifically, their partitional behaviour. Simplifying assumptions include single on/off activation of entire muscles or semi-arbitrarily defined mechanical elements. These limitations stem from the historical methodological approach to bipolar surface electromyogram recordings for inferring the intricate behaviour of the individual motor units involved in muscle activation. In fact, to date, the inclusion of motoneuron behaviour from the shoulder muscles in neuromechanical models remains elusive (Hughes & An, 1997). Therefore, shoulder models must rely on indirect measures of neural control, using metrics that only partially capture the complexity of muscle activation strategies (Farina *et al.*, 2010; Lulic-Kuryllo *et al.*, 2021*a*).

Classically, the approach to assessing muscular neural control has been global bipolar surface electromyography (EMG), using amplitude measures to infer neuromuscular adaptations to specific actions with applications in biomechanics (Lawrence & De Luca, 1983; Woods & Bigland-Ritchie, 1983; Hermans *et al.*, 1999; Day & Hulliger, 2001; Karlsson & Gerdle, 2001; Keenan *et al.*, 2005; Farina *et al.*, 2010). However, the specificity of EMG amplitude in inferring neural drive to the muscle remains debated (Christie *et al.*, 2009; Farina *et al.*, 2010). Amplitude cancellation of surface motor unit action potentials is a key factor affecting the relationship between EMG amplitude and neural drive (Yao *et al.*, 2000; Day & Hulliger, 2001; Dimitrova & Dimitrov, 2003; Keenan *et al.*, 2005), because as additional motor units may be recruited during the gradation of force, the superposition of positive and negative phases of action potentials could result in a non-proportional increase in EMG amplitude (Day & Hulliger, 2001; Keenan *et al.*, 2005). Additionally, bipolar EMG provides only muscle activity in the recording volume of the electrodes (i.e., local information). In the case of the shoulder, where large muscles produce complex actions across multiple degrees of freedom, not all muscle portions may be either monitored or active during all actions (i.e., within-muscle localized activation) (Lulic-Kuryllo *et al.*, 2021*a*) via standard bipolar surface EMG. For instance, previous evidence suggested that localized regions of the deltoid, pectoralis major, and latissimus dorsi can be activated based on the specific shoulder action direction (Wickham & Brown, 1998, 2012; Brown *et al.*, 2007; Lulic-Kuryllo *et al.*, 2022). Finally, when recording myoelectric signals with global bipolar EMG, the risk of crosstalk must be considered. Signals generated by secondary muscles may lead to the erroneous interpretation of myoelectric signals from the primary muscle under investigation (De Luca & Merletti, 1988). Therefore, caution must be taken when assessing muscle activity using bipolar global signals, given the possibility of cancellation or crosstalk in the myoelectric recordings.

Advancements in myoelectric recordings in the early 1980's have led to high-density surface electromyograms (HDsEMG) (Masuda *et al.*, 1983, 1985; Reucher *et al.*, 1987; Merletti *et al.*, 1999). The benefit of recording with the evolving HDsEMG technology is its non-invasive nature and the ability to provide the spatial distribution of activation within and across muscles during complex actions. Additionally, when combined with motor unit decomposition algorithms (Holobar & Zazula, 2007; Ning *et al.*, 2015; Chen & Zhou, 2016; Negro *et al.*, 2016), the approach has the potential to record a large number of concurrently discharging motoneurons during voluntary contractions (Inglis *et al.*, 2025). As the alpha motoneuron is the final common pathway of the neuromuscular system, integrating synaptic inputs from spinal and supraspinal pathways (Liddell & Sherrington, 1925; Sherrington, 1925), the analysis of motor unit discharge behaviour provides an effective way to assemble information on the generation and control of actions. A recent systematic review and meta-analysis revealed that most motor unit behaviour investigations have focused on the lower rather than the upper-body, leading to a paucity of data on the upper limb (Inglis *et al.*, 2025). Additionally, it was revealed that of the upper limb muscles, specifically major movers of the shoulder, there are few motor unit behaviour studies investigating the *upper trapezius* (Westgaard & De Luca, 2001; Falla & Farina, 2008*a*, 2008*b*; Gerdle *et al.*, 2008; Holobar *et al.*, 2009; Dideriksen *et al.*, 2016; Kirk *et al.*, 2019) and *pectoralis major* (Lulic-Kuryllo *et al.*, 2021*b*) using invasive or non-invasive techniques, none that examined the *latissimus dorsi* (Padovan *et al.*, 2024) and only three examining the *deltoid* (De Luca *et al.*, 1982; Doherty & Stashuk, 2003; Baslo *et al.*, 2024), which all used intramuscular electrodes (Joseph *et al.*, 2019).

Therefore, the aim of this paper was to develop a novel methodological framework to investigate four isometric shoulder actions (abduction, adduction, flexion and extension) at two shoulder elevation angles to fully assess and compare the neural control of the superficial

shoulder muscles (deltoid, clavicular pectoralis major, upper trapezius and latissimus dorsi) at the global activation level (average HDsEMG amplitude), the spatial distribution of activation level (coefficient of variation of the HDsEMG amplitude maps) and the motor unit level (discharge patterns). For this, we combined a six-degree-of-freedom load cell with a robotic arm with the evolving HDsEMG technology. Additionally, this paper provides several examples of the type of extractable neural shoulder control information within the proposed framework. The novel framework proposed aims to establish guidelines for future investigations of the shoulder complex's large muscles and to advance shoulder musculoskeletal modelling.

2.0 METHODS

2.1 Participants

Six healthy individuals free of any musculoskeletal or neuromuscular abnormalities (1 female; mean ± SD: age 28 ± 4 years; height 180 ± 7 cm; mass 79 ± 9 kg) voluntarily participated. All participants provided written informed consent before starting the experiments that conformed to the standards set by the latest version of the Declaration of Helsinki, which was approved by the ethics committee of the Università degli Studi di Brescia (code NP5890).

2.2 Experimental protocol

2.2.1 Experimental setup

Each participant visited the lab on a single day where, in a randomized order, they performed multiple degree-of-freedom isometric contractions in a 2-hour session. Participants were seated in a rigid testing chair with their hip and knee joints at 90° of flexion (0° indicates full extension) and a broad Velcro® strap placed around the midsection to minimize lateral torso movements. The participant's arm was extended and placed slightly (<20°) in the scapular plane to avoid discomfort when performing the selected actions. The participants'

upper arm was placed into a custom-built testing jig manufactured from rectangular metal tubing to ensure a rigid transfer of forces produced to the load cell (**Figure 1b**). The testing jig was attached to a 6-degrees of freedom load cell (© 2025 Advanced Mechanical Technology Inc., Watertown MA, USA, model #MC3A) to measure force output (**Figure 1c**). The load cell has a capacity of F_x, F_y of 225 N and F_z of 445 N, and a sensitivity of F_x, F_y of 5.4 μV/V-N and F_z of 1.35 μV/V-N. The load cell was attached to a robotic arm (Kawasaki Robotics Inc., Wixom MI, USA; **Figure 1a**) with a custom-machined aluminium coupling (**Figure 1d**). The importance of implementing the robotic arm was to position the testing jig and load cell through fine adjustments to accommodate individual anatomical landmarks, ensuring participants performed each action in identical relative positions and enabling precise recording of the forces produced during each action. Once positioned, the robotic arm was switched off and disconnected from all electrical sources to minimize electrical interference in the EMG signal.

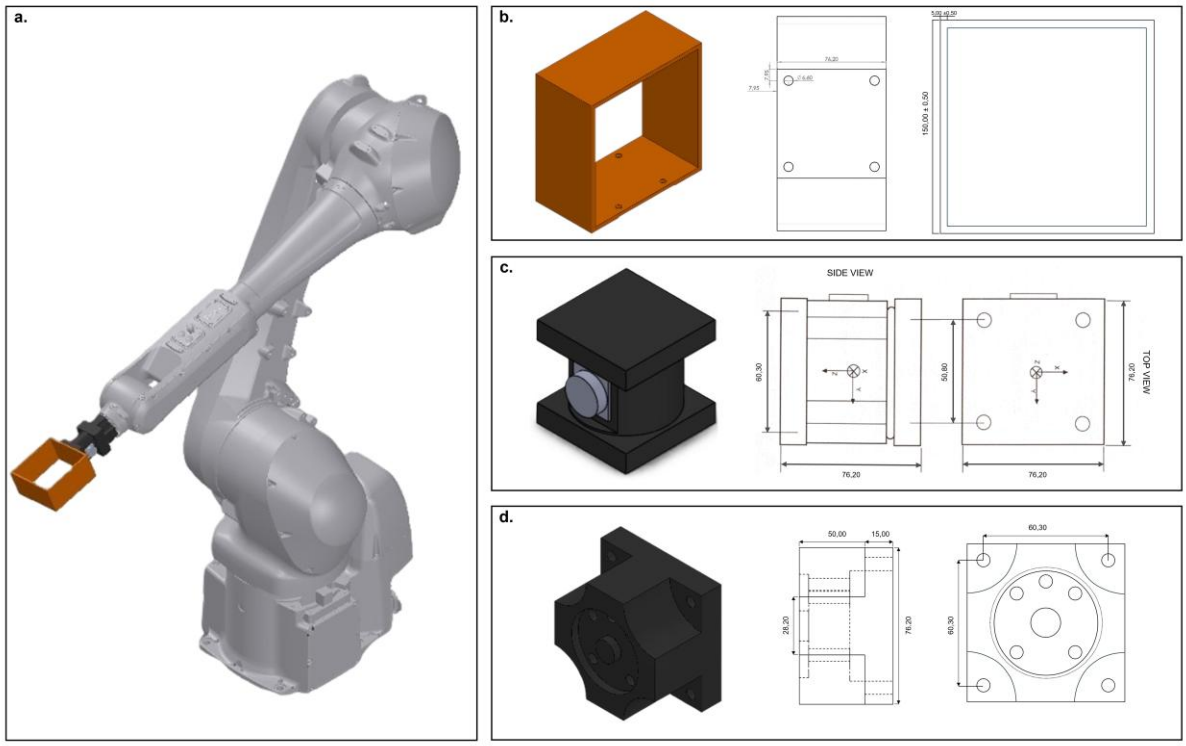

Figure 1. Mechanical components designed and manufactured for the robotic setup *(a) Complete robot assembly showing the robot with all components mounted. (b) 3D model and 2D technical drawings of the jig. (c) 3D model and 2D technical drawings of the six degree-of-freedom load cell. (d) 3D model and 2D technical drawings of the coupling between the robotic arm and the load cell. Measurements are reported in millimetres (mm).*

182 *2.2.2 Experimental tasks*

183 Each participant performed four isometric contractions at 30° and 65° of lateral
184 shoulder abduction. The actions were: abduction, adduction, flexion and extension. **Figure 2**
185 illustrates the position of the participant during the four actions across two shoulder angles. In
186 **Figure 2**, the direction of the force vector is depicted with arrows for each action. Each action
187 was performed at two shoulder angles to alter the deltoid muscle length (30° long; 65° short)
188 and optimize the angles where the deltoid can initiate action during abduction (Peterson &
189 Rayan, 2011).

190 All experimental actions were repeated twice for each action and shoulder angle,
191 resulting in a total of 16 trials (4 actions × 2 shoulder angles × 2 trials). Prior to each condition
192 (angle/action), participants performed three voluntary maximum isometric contractions
193 (MVCs) for 3-5 s, with a 3-min rest between each bout. The greatest value across the three
194 MVCs was the maximal isometric shoulder force output for the individual condition and was
195 used as a reference to set the target for the submaximal contractions.

196 Subsequently, participants underwent a short familiarization period, during which they
197 were instructed to exert isometric shoulder forces at 10% MVC for approximately 10 s. This
198 familiarization task was repeated up to a maximum of five times to ensure that participants
199 could maintain the force output as steadily as possible at a target level, which was visually
200 assessed by a researcher (JGI). Following the familiarization period, participants were
201 instructed to perform two isometric contractions following a trapezoidal profile. The
202 trapezoidal profile involved a linear increase at a rate of 3% MVC/s, a plateau phase for 30 s,
203 and a linear decrease at a rate of 3% MVC/s. The target force output was set at 30% MVC (i.e.,
204 moderate force output) to mimic common outputs during activities of daily living (Lulic-
205 Kuryllo *et al.*, 2021*a*).

206

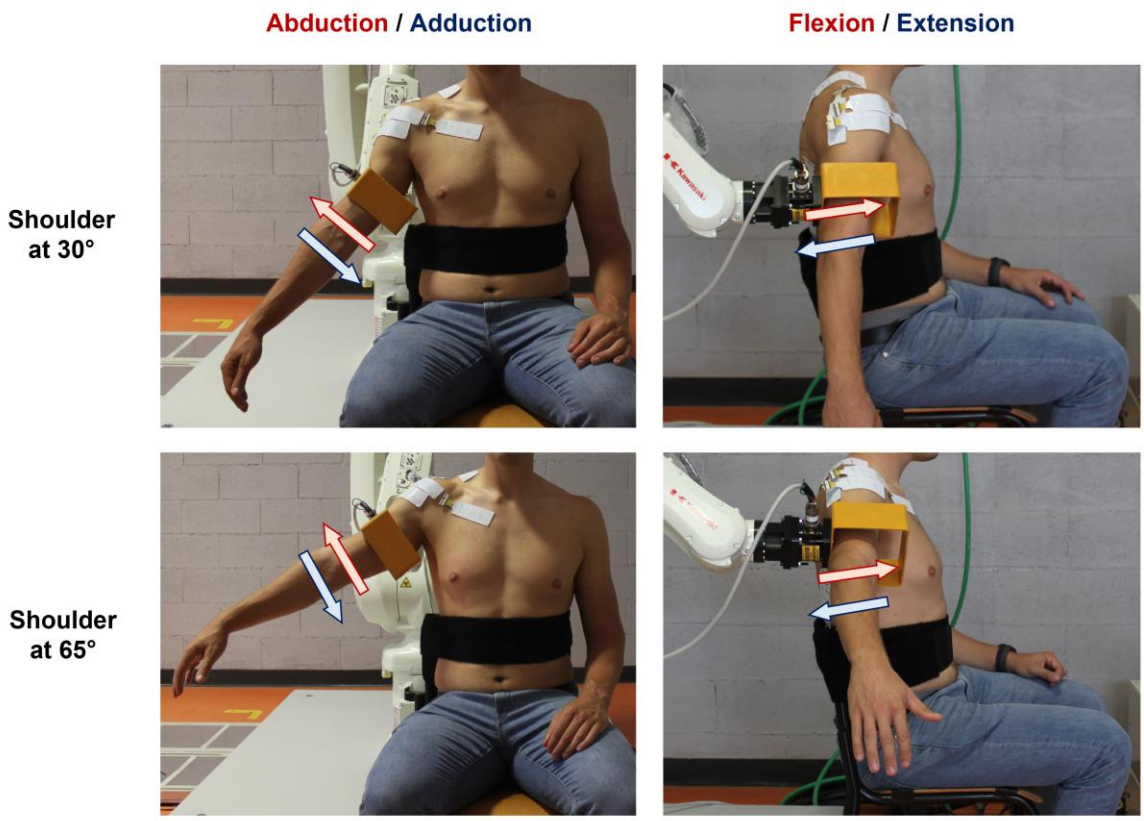

Figure 2. Experimental Actions. *Shoulder abduction/adduction (left, anterior view) and flexion/extension (right, lateral view) performed at 30° (top) and 65° (bottom) of shoulder abduction. The arm was secured to a passive robotic interface, which secured the participant in position for each given action. A broad black Velcro® strap was placed around the midsection and secured to the testing chair to minimize actions of the trunk.*

2.2.3 Force feedback

A novel graphical user interface (GUI) was developed in MATLAB (version 2024a) to provide visual feedback of the force output and the rate at which the force was to be developed during the trapezoidal profile (**Figure 3e**). Force feedback was provided based on the axis being investigated relative to the three-axis load cell connected to the PC by an A-D board (National Instruments CORP., NI USB-6343). The selected axis was represented by either a horizontal or vertical line, where the Y direction was utilized for abduction and adduction, and the Z direction during flexion and extension (frontal) relative to the load cell. The GUI provided a green target box with the dimensions set to ± 2.5% MVC and a blue circle to represent the changes in force output. Each participant was instructed to maintain the blue circle inside the

223 square. In cases where the error in force production exceeded 2.5% MVC, the square would
224 turn red, and the participant would be encouraged to adjust the force output to meet the target
225 force. Visual feedback was displayed on a monitor placed 1.3 meters in front of the participant
226 at eye level.

227 ***2.3 Data collection***

228 HDsEMG were acquired from the four major humeral movers (anterior, lateral and
229 posterior deltoid, clavicular pectoralis major, upper trapezius, and latissimus dorsi) during the
230 submaximal isometric actions using six two-dimensional adhesive arrays (HD08MM1305 and
231 HD08MM1606; 1 mm diameter; 8 mm inter-electrode distance; OT Bioelettronica, Turin,
232 Italy). The arrays placed over the deltoid and clavicular pectoralis major (see below) consisted
233 of 64 electrodes arranged in 13 rows by 5 columns, with one missing channel in the top left
234 corner. As for the upper trapezius and the latissimus dorsi, the arrays consisted of 96 electrodes
235 arranged in 16 rows by 6 columns. Prior to array and reference electrode placement, the area
236 was shaved, mildly abraded (EVERI, Spes Medica, Genova, Italy), cleaned with distilled water,
237 and dried with paper towel. The electrode-skin contact was ensured by filling the foam cavities
238 with conductive paste (AC cream, Spes Medica, Genova, Italy). Two reference electrodes were
239 used; one positioned on the right elbow (electrode strap) at the level of the epicondyles and the
240 other on the acromion process (snap electrode).

241 Several arrays and configurations were piloted to achieve the greatest motor unit yield
242 in the deltoid (see appendix A). For the anterior/lateral deltoid, the electrode was placed
243 approximately 2 cm distal to the proximal deltoid tendon, starting from the anterior border
244 horizontally towards the posterior portion perpendicular to the insertion of the lateral fibres to
245 the humerus (*array 1*, **Figure 3a**). To cover more of the anterior and lateral aspects of the
246 deltoid, a second array was placed distally and slightly offset (2 array columns) and parallel to
247 the proximal array (*array 2*, **Figure 3a**). For the posterior deltoid, the electrode array was

positioned in line with the posterior aspect of the deltoid adjacent to the distal deltoid array (*array 3*, **Figure 3a**). For the clavicular region of the pectoralis major, the electrode array was placed approximately 2 cm inferior to the clavicle (superior *array* in (Lulic-Kuryllo *et al.*, 2021*a*); *array 4*, **Figure 3b**). For the upper trapezius, the electrode array was positioned to bisect the 7th and 8th row (*array 5*, **Figure 3c**) along a line drawn between C7 and the lateral edge of the acromion. This was done because of the use of the 96-electrode array which is larger (3 extra rows and 1 extra column) than the standard 64 electrode array used for the deltoid and clavicular pectoralis major above (modified from (Falla & Farina, 2008*b*). For the latissimus dorsi, a line was drawn approximately 3 cm inferior to and horizontal to the posterior axillary crease and parallel to the superior aspect of the iliac crest. From these lines, a diagonal line was drawn to follow the latissimus dorsi muscle fibres, and the array was placed in the middle of this area, ensuring that the majority of the array covered the bulk of the muscle (Padovan *et al.*, 2024) (*array 6*, **Figure 3d**).

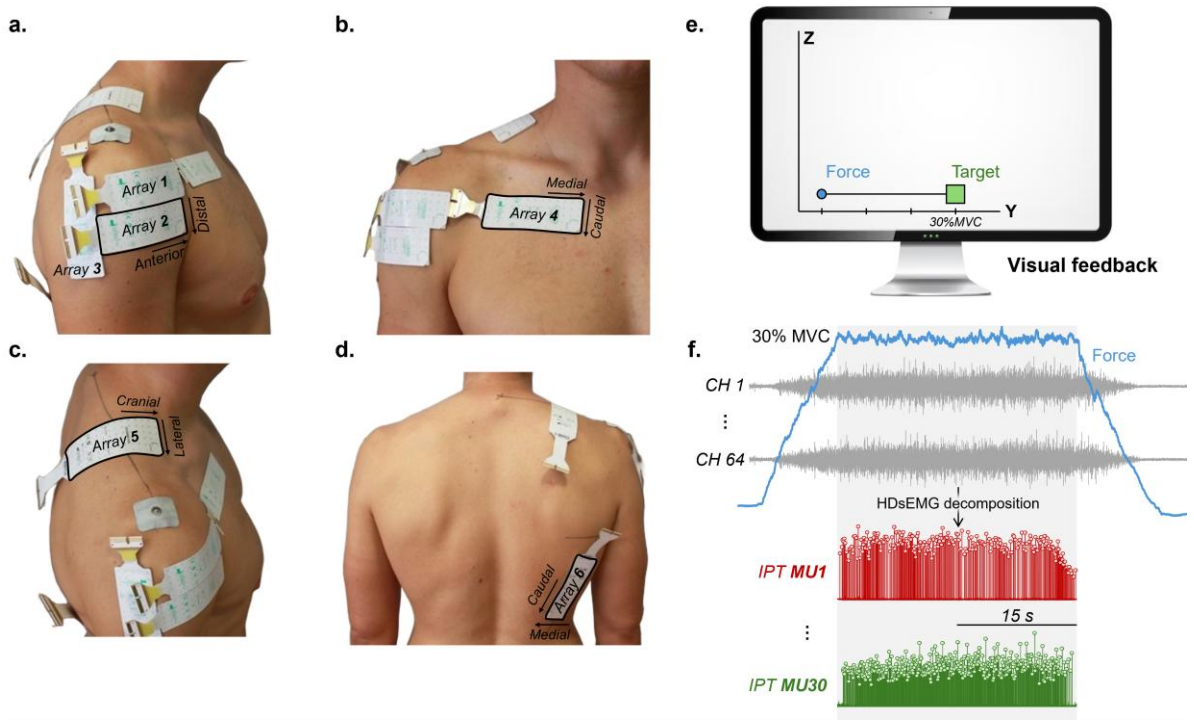

Figure 3. Electrode placement, visual feedback and HDsEMG analysis. *(a) Electrode placement for the deltoid. Array 1 was positioned horizontally approximately 2 cm distal from the insertion of the deltoid tendon. Array 2 was placed distally and slightly offset to cover the lateral and anterior deltoid. Array 3 was positioned vertically adjacent to the distal deltoid array. (b) Electrode placement for the clavicular region of the pectoralis major. Array 4 was positioned horizontally and approximately 2 cm inferior to the clavicle, avoiding the sternum. (c) Electrode placement of the upper trapezius. Array 5 was positioned to bisect the 7th and 8th row of the array along the line between C7 and the acromion process. (d) Electrode placement of the latissimus dorsi. Array 6 was positioned diagonally in an area delimited by two horizontal lines, drawn approximately 3 cm inferior to the posterior axillary crease and parallel to the superior aspect of the iliac crest, the array was placed in line with the muscle fibres. (e) Visual feedback of the force output. Visual feedback was provided from a line, a square box and a circle representing the profile, the target force and the force output of the participant, respectively. (f) Schematic representation of the HDsEMG decomposition. HDsEMGs were visually inspected and, subsequently, decomposed into motor unit innervation pulse train (IPTs). The 30-s plateau phase was considered for this analysis (light grey rectangle).*

HDsEMG and force outputs were digitized synchronously at a sampling frequency of 2000 Hz using a 16-bit A/D converter (10-500 Hz bandwidth; Novecento+, OT Bioelettronica, Turin, Italy). HDsEMG signals were recorded in monopolar derivation and amplified (8 V/V) to maximize signal resolution while avoiding saturation.

2.4 Data analysis

HDsEMG recordings were analysed offline in MATLAB (version 2024a) using custom-written scripts. As potential applications of the developed novel experimental framework, analyses were performed at the global activation level (average HDsEMG amplitude), the spatial distribution of activation level (coefficient of variation of the HDsEMG amplitude maps) and the motor unit level (discharge patterns) to assess the neural control of shoulder muscles. For all analyses, the 30-s plateau phase of each contraction was evaluated. HDsEMG were bandpass filtered between 20 and 900 Hz using a third-order Butterworth filter and subsequently visually inspected to identify and remove bad channels due to electrode-skin contact issues or artifacts (mean ± SD: 2 ± 1 channels removed across all actions and shoulder angles).

296 *2.4.1 HDsEMG root-mean-square amplitude and coefficient of variation*

297 To assess the global activation of the investigated muscles, the root-mean-square
298 (RMS) amplitude was utilized. Initially, single-differential (bipolar) EMGs were calculated as
299 the algebraic difference between monopolar signals detected by consecutive rows of electrodes.
300 Then, the RMS amplitude was calculated for each of the 59 (64-electrodes array) and 80 (96-
301 electrodes array) single-differential channels over the duration of the trial, generating
302 topographic maps of activation. The RMS amplitude maps were normalized to the average
303 RMS value obtained from a 250 ms window, centred around the peak maximum isometric
304 voluntary contraction, which was identified by a trained researcher (SR). RMS normalization
305 was repeated for each muscle, action, and shoulder angle. For simplicity, only *array 2* of the
306 deltoid was analysed. The average normalized RMS amplitude across all channels was then
307 considered as the global RMS amplitude of the muscle for each action and shoulder angle.

308 To assess the variability in spatial distribution of the muscle activation, the coefficient
309 of variation (CoV) of the normalised RMS amplitude maps was calculated (i.e., the standard
310 deviation of the normalized RMS amplitudes divided by their mean). The CoV was calculated
311 separately for each muscle, movement, and shoulder angle.

312 *2.4.2 HDsEMG decomposition*

313 HDsEMG signals were completely decomposed into their constituent motor unit spike
314 trains using a convolutive blind-source separation algorithm (Negro *et al.*, 2016). Briefly, after
315 extending and whitening the HDsEMG myoelectric signals, a fixed-point algorithm that seeks
316 sources that maximize a measure of sparsity was applied to identify the motor unit spike trains
317 (**Figure 3f**). The spikes were separated from the noise using the K-means algorithm and, while
318 iteratively updating the motor unit separation vectors, the discharge times estimation was
319 further refined by minimizing the coefficient of variation of the inter-spike intervals. This
320 decomposition method has been previously validated (Negro *et al.*, 2016) and extensively

321 applied to assess the activity of single motor units (Negro *et al.*, 2016; Cogliati *et al.*, 2020;
322 Cabral *et al.*, 2024). After the automatic identification of motor units, any missed or
323 misidentified motor unit discharges that produced non-physiological discharge rates (< 4 pulses
324 per second or > 50 pulses per second; Negro *et al.*, 2009) were manually identified and
325 iteratively edited by an experienced operator (JGI, SR, CC), and the subsequent motor unit
326 spike trains were re-estimated (Martinez-Valdes *et al.*, 2017; Hassan *et al.*, 2020). This
327 approach has been shown to be highly reliable across operators (Hug *et al.*, 2021). Only motor
328 units with a silhouette (SIL) value, which is a quality control measure of the decomposition
329 accuracy, greater than 0.87 were included in the further analysis (Negro *et al.*, 2016).

330 *2.4.3 Motor unit discharge behaviour*

331 The instantaneous discharge rates of each identified motor unit were determined by
332 computing the inverse of the inter-spike intervals, and subsequently, the mean discharge rate
333 was calculated and considered for further analysis.

334 *2.4.4 Motor unit action potential amplitude*

335 To assess the spatial distribution of motor unit action potentials (MUAP), templates
336 were obtained using the spike-triggered averaging technique (Stein *et al.*, 1972). Specifically,
337 single-differential EMGs were segmented into 100-ms windows centred on the discharge times
338 of individual motor units and averaged. The peak-to-peak amplitude of each template was then
339 calculated across channels, generating topographical MUAP amplitude maps. These maps
340 were used both to validate the decomposed motor units and to exemplify the type of neural
341 information that can be extracted with the proposed framework. As for the HDsEMG
342 normalized RMS amplitude analysis, only *array 2* of the deltoid was analysed.

343 ***2.5 Statistical analysis***

All statistical analyses were performed in R (version 4.2.2), using the RStudio environment. Linear mixed-effect models (LMM) were applied for all statistical analyses, as they account for the non-independence of data points within each participant, which is particularly relevant for motor unit data. To compare global normalized RMS amplitude, CoV of RMS amplitude maps and motor unit mean discharge rate, random intercept models were applied with action (abduction, adduction, flexion and extension) and muscle (deltoid, clavicular pectoralis major, upper trapezius and latissimus dorsi) as the fixed effects and participant as the random effect (e.g., *mean discharge rate ~ 1 + action*muscle + (1 | participant)*). LMMs were implemented using the package *lmerTest* (Kuznetsova *et al.*, 2017) with the Kenward-Roger method to approximate the degrees of freedom and estimate the *p*-values. The *emmeans* package was used, when necessary, for multiple comparisons and to determine estimated marginal means with 95% confidence intervals (Lenth *et al.*, 2019). All individual data of motor unit discharge times are available at https://doi.org/10.6084/m9.figshare.30999811.

3.0 RESULTS

3.1 HDsEMG root-mean-square amplitude and coefficient of variation

Figure 4a depicts the topographical maps of the RMS amplitude at the 30° shoulder angle across muscle and actions for a selected participant. During abduction, the deltoid was the most active muscle, particularly in the lateral-anterior portion of *array 2* (see **Figure 3a**), followed by the caudal region of the upper trapezius. As for the clavicular pectoralis major and latissimus dorsi, during abduction, there was no visual evidence of significant activation. During adduction, most of the activity was in the latissimus dorsi and covered much of the array, followed by a small amount of activity in the medial-caudal portion of the clavicular pectoralis major array. However, there was no evident activity in the deltoid and upper trapezius during the adduction action. During flexion, the activity was predominantly in the

anterior deltoid, followed by the clavicular pectoralis major. As for extension, the deltoid was again the most active, with the activity primarily towards the posterior aspect of the array. There was also significant activity in the caudal region of the array in the latissimus dorsi and upper trapezius, with no evidence of activity in the clavicular pectoralis major. In **Figure 4b,** the topographical RMS amplitude maps for the same selected participant are depicted, but at a shoulder angle of 65°. The activation patterns during abduction, adduction, and flexion closely resembled those reported above for the 30° condition. However, during extension, the deltoid was significantly active across *array 2*. Additionally, as seen for the 30° condition, a significant amount of activity was observed in the caudal region of the upper trapezius, but with little activity in the latissimus dorsi.

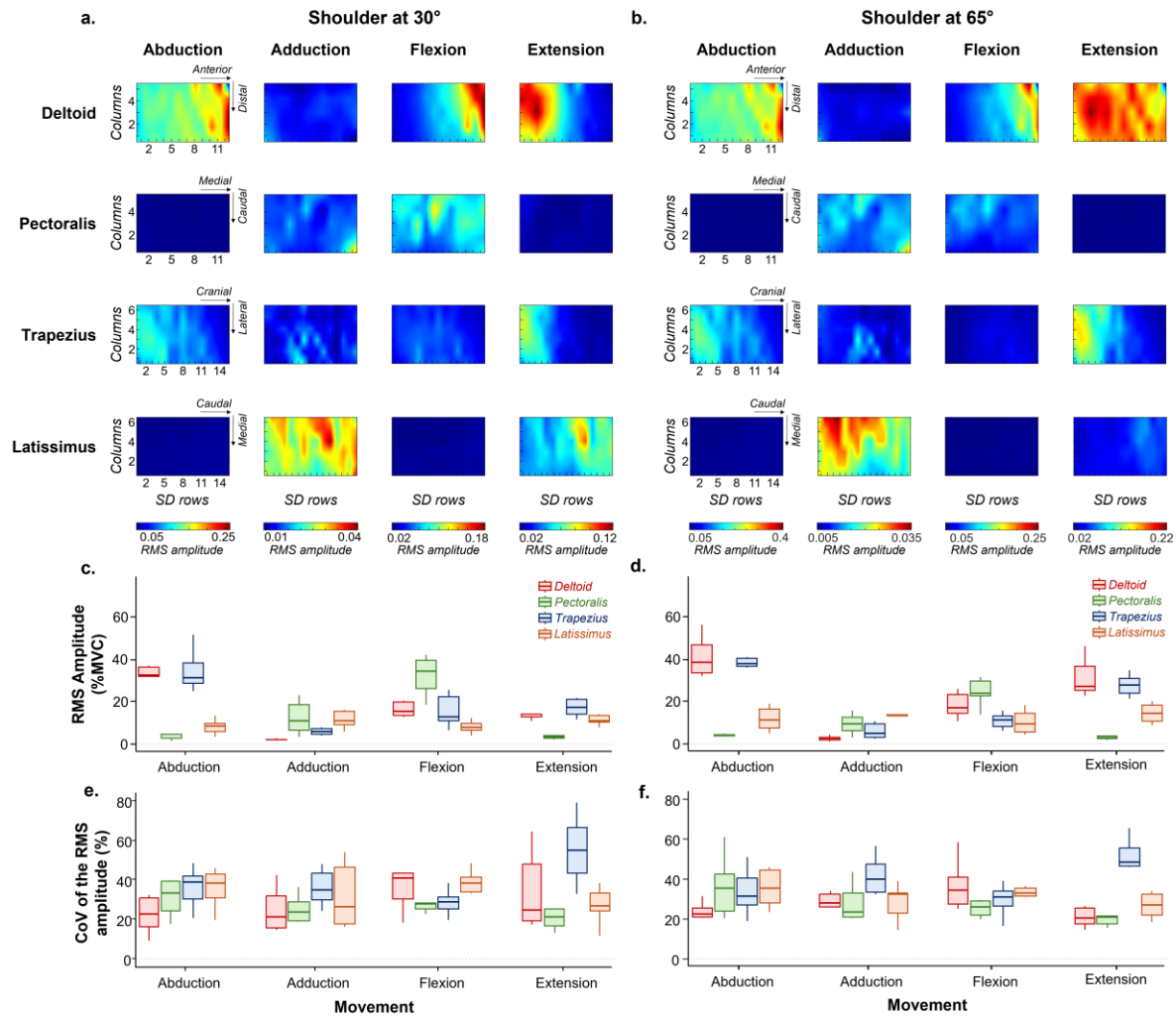

Figure 4. Muscle activation patterns across shoulder actions at 30° and 65°. *RMS amplitude topographical maps for the deltoid, clavicular pectoralis major, upper trapezius, and*

latissimus dorsi during abduction, adduction, flexion and extension. These actions were performed with the shoulder positioned at 30° (a) and 65° (b) of lateral abduction. The x- and y-axes represent the rows and columns of the array, with colour intensity (from dark blue to dark red) indicating the level of muscle excitation. Panels (c) and (d) show the group results of the global normalized RMS amplitude (%MVC) for each action and muscle. Panels (e) and (f) show the group result of the coefficient of variation (CoV) of the RMS amplitude maps. Horizontal traces, boxes, and whiskers represent the median value, interquartile interval, and distribution range, respectively.

Figures 4c and **4d** show the group results for the global normalized RMS amplitude at 30° and 65° shoulder angles. For both 30° and 65° there were statistically significant interactions between muscle and action (30°: LMM, F=20.030, p<0.001; 65°: LMM, F=28.213, p<0.001). The following pairwise comparisons were common for both angles. For abduction, the deltoid and the upper trapezius had a significantly greater global normalized RMS amplitude compared to clavicular pectoralis major and latissimus dorsi (p<0.001 for all comparisons). During flexion, the normalized RMS amplitude of the clavicular pectoralis major was significantly greater compared to upper trapezius and latissimus dorsi (p<0.001 for all comparisons). Additionally, at the 30° shoulder angle, during flexion the normalized RMS amplitude of the clavicular pectoralis was significantly greater than the deltoid (p<0.001). During extension, both the deltoid (p=0.022) and the upper trapezius (p<0.001) had a greater normalized RMS amplitude compared to the clavicular pectoralis major, with no significant differences compared to the latissimus. When comparing the same muscle across actions at the 30° and 65° shoulder angle, the deltoid normalized RMS amplitude was significantly greater in abduction, flexion, and extension compared to adduction (p<0.01 for all comparisons), as well as during abduction compared to flexion and extension (p<0.01 for both comparisons). During flexion the clavicular pectoralis major exhibited the greatest normalized RMS amplitude compared to all other actions (p<0.001 for all comparisons). As for the upper trapezius, the normalized RMS amplitude was significantly greater during abduction compared to adduction, flexion, and extension (p<0.001 for all comparisons). Finally, the latissimus dorsi was not significantly different across all actions (p>0.05 for all comparisons).

411 The group results for the CoV of the normalized RMS amplitude maps at the 30° and
412 65° shoulder angle showed a statistically significant interaction between muscle and action
413 (**Figure 4e and 4f**, 30°: LMM, F=2.790, p=0.007; 65°: LMM, F=2.789, p<0.001). The
414 following pairwise comparisons were common for both angles. For abduction, adduction, and
415 flexion there were no significant differences observed across muscle (p>0.05). During
416 extension, the CoV of the normalized RMS amplitude maps of the upper trapezius was
417 significantly greater compared to all other muscles (p<0.05 for all comparisons). While
418 comparing the same muscle across movement, at the 30° shoulder angle, the upper trapezius
419 had a significantly greater CoV of the normalized RMS amplitude maps during extension
420 compared to all other movements (p<0.05 for all comparisons). While, at the 65° shoulder
421 angle, the upper trapezius CoV of the normalized RMS amplitude maps was significantly
422 higher during extension compared to flexion (p=0.030).

423 ***3.2 Motor unit discharge behaviour***

424 **Figures 5** through **8** illustrate, for the different shoulder actions at the 30° shoulder
425 angle, the neural features at the motor unit level that can be extracted using the proposed novel
426 framework. For each muscle, representative MUAP amplitude maps and the corresponding
427 motor unit instantaneous discharge rate are presented. During abduction (**Figure 5**), motor
428 units could be identified only in the deltoid and upper trapezius for this representative
429 participant, with 30 and 19 units decomposed, respectively. For the deltoid, the motor units
430 were distributed across different regions of *array 2*, including anterior (MUAP 1 and MUAP
431 30), lateral (MUAP 3 and MUAP 5), and posterior regions (MUAP 2 and MUAP 4). In contrast,
432 most of the motor units identified in the upper trapezius were located cranially within the array.
433 Additionally, as seen in the right panel of **Figure 5**, most of the motor units identified from
434 both muscles were tonically active throughout the plateau phase of the action.

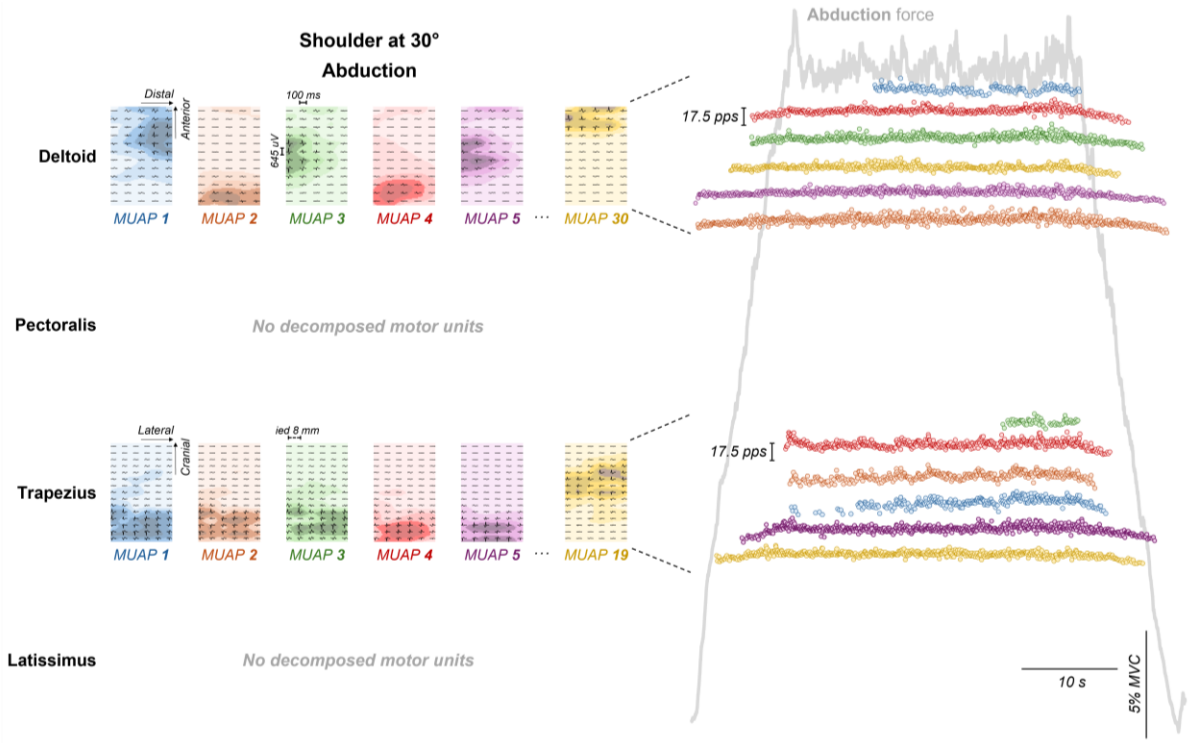

Figure 5: Motor unit action potential amplitude maps and motor unit discharge rate during shoulder abduction at 30°. *Motor unit action potentials were obtained using the spike-triggered averaging technique from array 2. For this representative subject, motor units were identified in the deltoid (30 units) and upper trapezius (19 units). No motor units were decomposed from the clavicular pectoralis major or latissimus dorsi (left panel). Abduction force profile (grey line), and motor unit instantaneous discharge rate are shown in the right panel. Separately per muscle, each motor unit is represented with a colour, used both for the MUAP distribution maps and the instantaneous discharge rate.*

Figure 6 is the same representative participant during the adduction action at a 30° shoulder angle. In this condition, motor units were identified in the deltoid (5 units), clavicular pectoralis major (16 units), upper trapezius (2 units), and the latissimus dorsi (13 units). The identified motor units in the deltoid were located across all regions of the deltoid. For the upper trapezius the identified units were located caudally and, in the latissimus, dorsi, as seen in the deltoid, the units were spread across the entire region. Interestingly, the units identified in the clavicular pectoralis major covered the entire *array*, however the majority of the activity following the clavicular pectoralis major line of action. While most of the clavicular pectoralis major and latissimus dorsi motor units were tonically active throughout the plateau phase, some deltoid and two motor units identified in the upper trapezius exhibited more phasic activity.

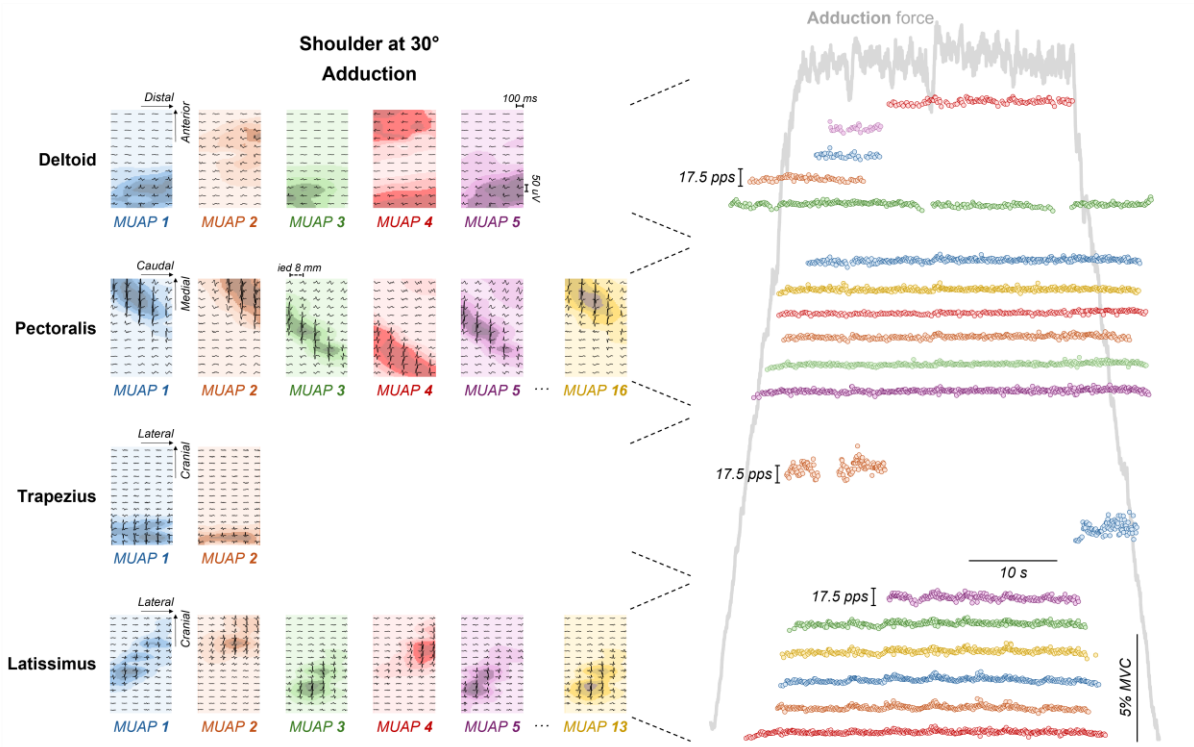

Figure 6: Motor unit action potential amplitude maps and motor unit discharge rate during shoulder adduction at 30°. *Motor unit action potentials were obtained using the spike-triggered averaging technique from array 2. For this representative subject, motor units were identified in the deltoid (5 units), clavicular pectoralis major (16 units), upper trapezius (2 units) and latissimus dorsi (13 units) (left panel). Adduction force profile (grey line), and motor unit instantaneous discharge rate are shown in the right panel. Separately per muscle, each motor unit is represented with a colour, used both for the MUAP distribution maps and the instantaneous discharge rate.*

Figure 7 shows the same representative participant during the flexion action at a 30° shoulder angle. In this condition, motor units were identified in the deltoid (20 units), clavicular pectoralis major (21 units), and upper trapezius (16 units), whereas again no motor units were identified in the latissimus dorsi. The identified motor units in the deltoid were predominantly located in the anterior region of the array (e.g., MUAP 1, MUAP 2, and MUAP 5). For both the upper trapezius and clavicular pectoralis major, motor units were distributed across different regions of their respective arrays. While most deltoid and clavicular pectoralis major motor units were tonically active throughout the plateau phase, some upper trapezius units exhibited more phasic activity.

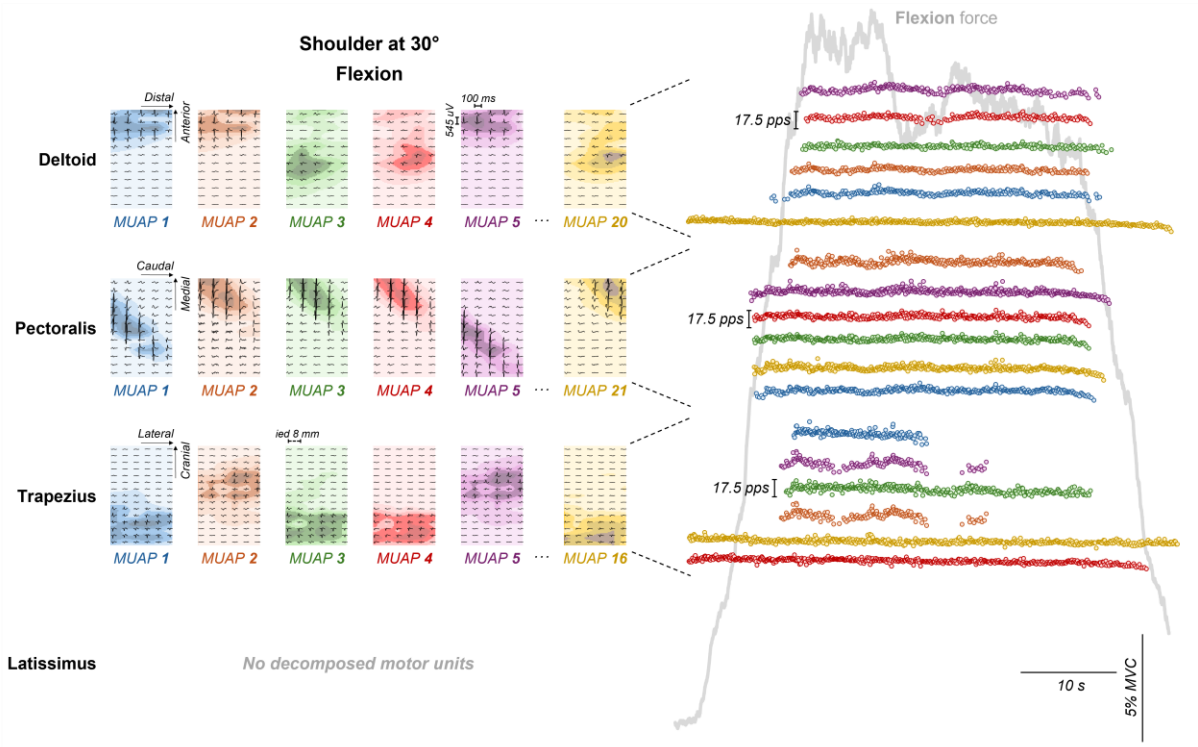

Figure 7: Motor unit action potential amplitude maps and motor unit discharge rate during shoulder flexion at 30°. *Motor unit action potentials were obtained using the spike-triggered averaging technique from array 2. For this representative subject (same as in Figure 5), motor units were decomposed from the deltoid (20 units), clavicular pectoralis major (21 units), and upper trapezius (16 units). No motor units were decomposed from the latissimus dorsi (left panel). The flexion force profile (grey line), and motor unit instantaneous discharge rate are shown in the right panel. Separately per muscle, each motor unit is represented with a colour, used both for the MUAP distribution maps and the instantaneous discharge rate.*

Figure 8 illustrates the same representative participant during the extension action at a 30° shoulder angle. In this condition, motor units were identified in the deltoid (9 units), upper trapezius (10 units), and latissimus dorsi (12 units), whereas no motor units were identified in the clavicular pectoralis major. The identified motor units in the deltoid were predominantly located in the posterior region of the array (e.g., MUAP 2, MUAP 3, and MUAP 9). For the upper trapezius, motor unit 1 was dispersed across the entire array, where the other motor units were located more caudally. In the latissimus dorsi, the motor units were distributed across different regions of the array with the majority located more cranially (e.g., MUAP 2, MUAP 4, MUAP 5, and MUAP 12). While most of the deltoid and upper trapezius motor units were tonically active throughout the plateau phase, the latissimus dorsi units exhibited both tonic and phasic activity.

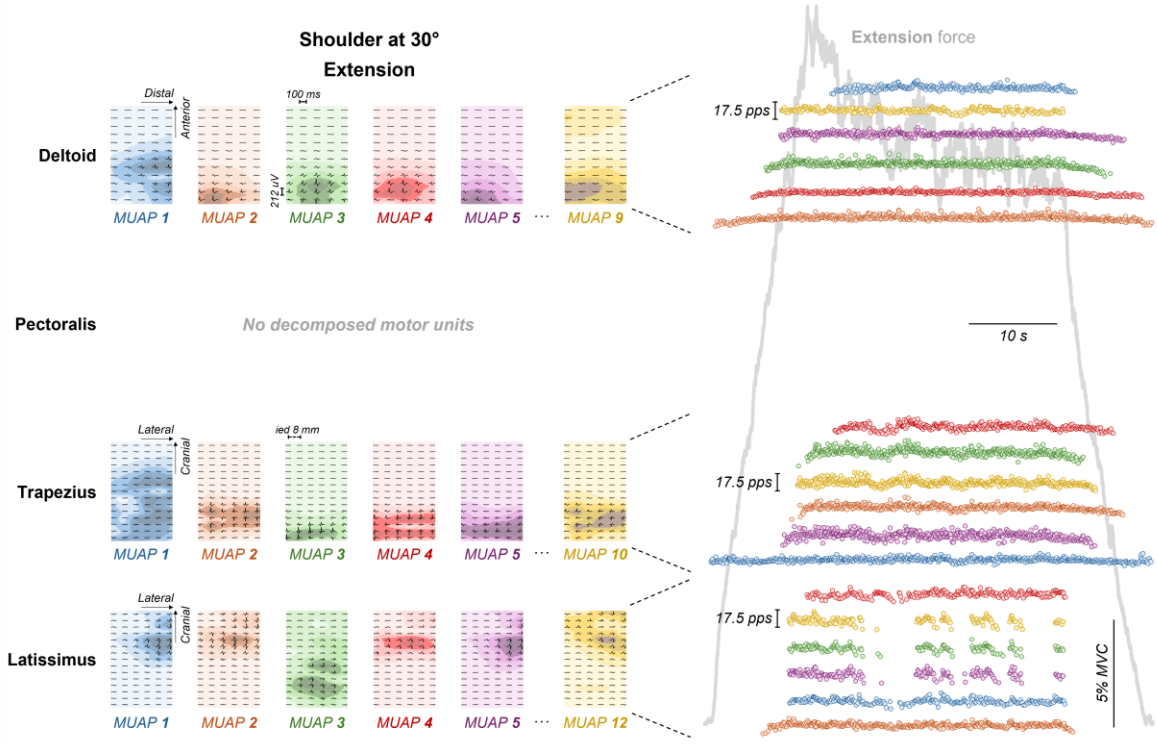

Figure 8: Motor unit action potential amplitude maps and motor unit discharge rate during shoulder extension at 30°. *Motor unit action potentials were obtained using the spike-triggered averaging technique from array 2. For this representative subject, motor units were identified in the deltoid (9 units), upper trapezius (10 units) and latissimus dorsi (12 units). No motor units were decomposed from the clavicular pectoralis major (left panel). Extension force profile (grey line), and motor unit instantaneous discharge rate are shown in the right panel. Separately per muscle, each motor unit is represented with a colour, used both for the MUAP distribution maps and the instantaneous discharge rate.*

Table 1 summarizes the motor unit yield across all muscles, actions, and shoulder angles. Overall, a greater number of motor units were decomposed at the 30° shoulder angle compared with 65°. Consistent with the representative case, no motor units were identified in the clavicular pectoralis major and latissimus dorsi during abduction, or in the latissimus dorsi during flexion. In addition, no units were decomposed from the clavicular pectoralis major during extension.

Table 1: *Average ± standard deviation motor unit yield across all muscles (deltoid, clavicular pectoralis major, upper trapezius and latissimus), actions (abduction, adduction, flexion and extension) and shoulder angles (30° or 65°).*

	SHOULDER AT 30 DEGREES				SHOULDER AT 65 DEGREES			
	Abduction	**Adduction**	**Flexion**	**Extension**	**Abduction**	**Adduction**	**Flexion**	**Extension**

Deltoid	12 ± 19	9 ± 15	10 ± 11	12 ± 7	7 ± 7	2 ± 3	10 ± 9	10 ± 11
Pectoralis	0 ± 0	5 ± 3	5 ± 7	0 ± 0	0 ± 0	6 ± 6	5 ± 6	0 ± 0
Trapezius	6 ± 6	5 ± 9	5 ± 5	5 ± 4	5 ± 3	3 ± 1	5 ± 2	4 ± 2
Latissimus	0 ± 0	5 ± 5	0 ± 0	3 ± 3	0 ± 0	3 ± 4	0 ± 0	2 ± 2

Figure 9 illustrates the group results for the mean motor unit discharge rate for the 30° (**Figure 9a**) and 65° (**Figure 9b**) shoulder angles. For both 30° and 65° there was a statistically significant interaction between muscle and action (LMM, F=3.190, p=0.008; LMM, F=6.821, p<0.001). The following pairwise comparison were common for both angles. For abduction, there were no significant differences between the mean motor unit discharge rate of the deltoid and upper trapezius (p>0.05). During flexion, at the 30° shoulder angle, the motor units of the clavicular pectoralis major had significantly higher mean discharge rate compared to the motor units of both upper trapezius and deltoid (p<0.05 for both comparisons). However, during flexion, at the 65° shoulder angle, both the deltoid and clavicular pectoralis major had significantly greater motor unit discharge rates compared to the upper trapezius (p<0.001 for both comparisons). For extension, both the deltoid and upper trapezius had significantly higher motor unit discharge rate compared to the latissimus dorsi (p<0.05 for both comparisons). When comparing the same muscle across actions at the 30° and 65° shoulder angles, the deltoid had a greater mean motor unit discharge rate during abduction, flexion and extension actions compared to adduction (p<0.001 for all comparisons). The mean motor unit discharge rate of the clavicular pectoralis major was higher during flexion than adduction (p<0.001), however, the upper trapezius mean motor unit discharge rate during abduction was greater compared to adduction and flexion (p<0.05 for both comparisons).

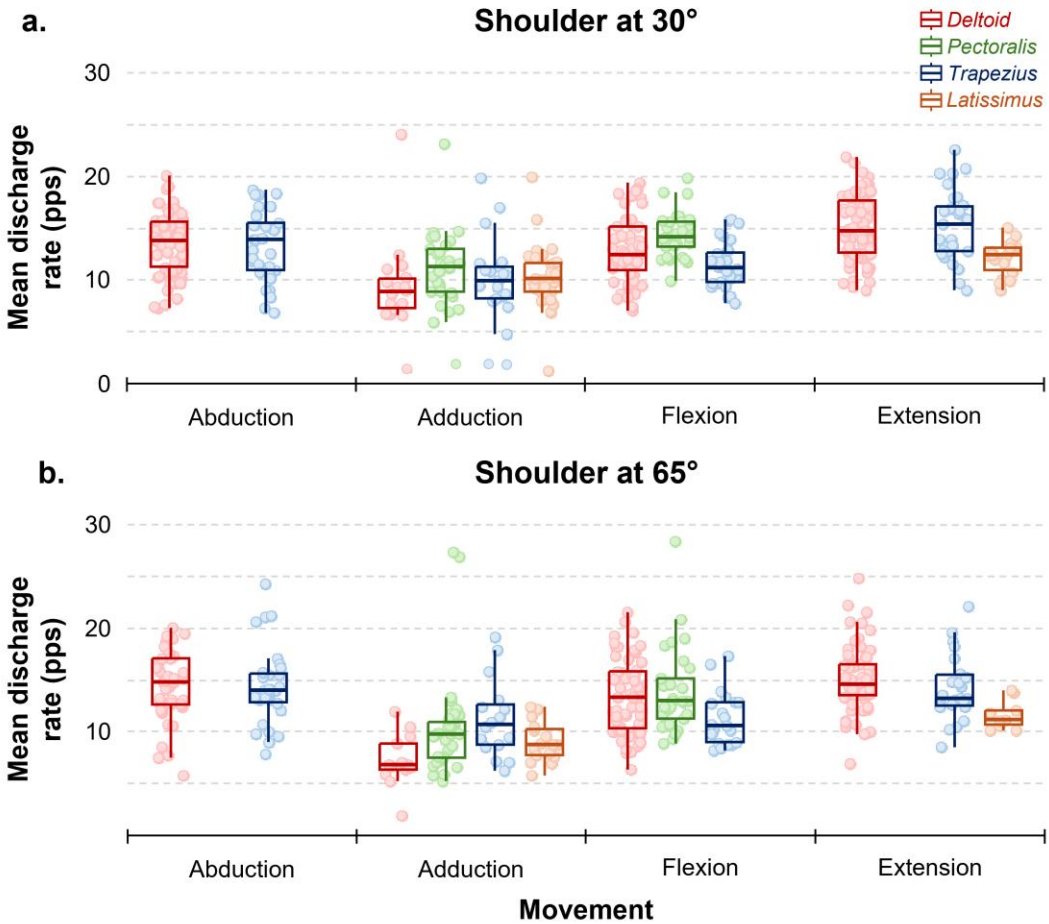

Figure 9: Motor unit discharge behaviour across actions and shoulder angles. *Group results for the mean motor unit discharge rate (a and b) during abduction, adduction, flexion, and extension at both 30° (top) and 65° (bottom) shoulder angles. Horizontal traces, boxes, and whiskers represent the median value, interquartile interval, and distribution range, respectively; individual circles correspond to single motor units.*

4.0 DISCUSSION

The aim of this methodological paper was to propose a novel framework based on the investigation of four isometric shoulder actions at two angles to fully assess the neural control of the superficial shoulder muscles (deltoid, clavicular pectoralis major, upper trapezius, and latissimus dorsi). This framework integrates information across multiple levels of analysis, including global HDsEMG amplitude (normalized RMS), spatial distribution of activation (CoV of RMS amplitude maps), and motor unit discharge behaviour (discharge statistics). To our knowledge, this is the first paper to report motor unit behaviour obtained with non-invasive

545 HDsEMG from the deltoid and latissimus dorsi, and to concurrently assess motor unit activity
546 across all four superficial shoulder muscles during controlled isometric actions. By combining
547 a six-degree-of-freedom load cell, a robotic arm, and evolving HDsEMG technology with
548 motor unit decomposition, the proposed framework demonstrates the feasibility of assessing
549 neural control of the shoulder musculature beyond traditional bipolar EMG approaches.
550 Importantly, this framework provides several examples of the type of extractable neural
551 information that can be obtained when global, spatial, and motor unit analyses are integrated,
552 thereby offering methodological guidelines for future investigations and contributing to the
553 advancement of shoulder neuromechanical and musculoskeletal modelling.

554 ***4.1 Differences across muscles within the same action***

555 The application of the proposed framework can be integrated into assessments from
556 many disciplines, including but not limited to, sport, physiotherapy and assessment of clinical
557 populations for exercise prescription and rehabilitation. The application of the framework in
558 clinical population, such as stroke and breast cancer survivors, has the ability to assist in
559 monitoring the progression of treatment or the potential negative effects of treatment
560 (Leonardis *et al.*, 2022). The proposed framework can be used in addition to assessments with
561 standard bipolar recordings, which has been shown to mischaracterize pectoralis major activity
562 in commonly performed tasks (Lulic-Kuryllo *et al.*, 2021*a*, 2023). Therefore, the additional of
563 HDsEMG recordings can provide critical information during assessments.

564 General consensus is that during complex shoulder actions, most of the muscles will
565 stabilize while others will produce the necessary muscle forces to initiate action (Schenkman
566 & Rugo de Cartaya, 1987; Kelly *et al.*, 2002). During shoulder abduction, both the deltoid and
567 upper trapezius exhibited significantly greater global RMS amplitudes compared to the
568 clavicular pectoralis major and latissimus dorsi, consistently across shoulder angles (**Figures**

569 **4c, 4d**). This pattern aligns with the primary mechanical roles of the deltoid in humeral
570 elevation and the upper trapezius in scapular stabilization during force generation (Paine &
571 Voight, 1993; Trudeau *et al.*, 2022). From a global EMG perspective, these two muscles would
572 therefore be interpreted as the dominant contributors to the abduction action. However, the
573 additional spatial and motor unit analyses revealed important nuances not captured by global
574 amplitude alone. Motor units identified in the upper trapezius were predominantly localized in
575 the caudal portion of the array (**Figures 5 through 8**), indicating a more spatially confined
576 activation strategy (Falla & Farina, 2008*b*). In contrast, the deltoid showed region-specific
577 activation, with motor units distributed across anterior, lateral, and posterior regions of the
578 array, reflecting the engagement of multiple functional compartments within the muscle
579 (**Figures 5 through 8**). Despite these distinct spatial recruitment patterns, the mean motor unit
580 discharge rates did not differ between the deltoid and upper trapezius (**Figures 5 through 8**).
581 This combination of findings suggests that, during abduction, differences between these
582 muscles might not be primarily driven by the magnitude of neural drive, but rather by how that
583 drive is spatially distributed within each muscle. These observations illustrate how the
584 proposed framework allows differentiation of muscle-specific control strategies within a single
585 functional action

586 During shoulder extension, the deltoid and upper trapezius again exhibited the greatest
587 global EMG amplitude, but this was accompanied by a marked increase in spatial heterogeneity
588 of activation in the upper trapezius, as reflected by a higher coefficient of variation of the RMS
589 amplitude maps (**Figure 4**). This region-specific activation of upper trapezius is in line with
590 previous studies showing higher caudal activation during shoulder actions (Falla & Farina,
591 2008*a*, 2008*b*). While global measures alone would suggest a secondary role of the upper
592 trapezius in this action, the spatial analysis indicates a more complex activation pattern,
593 potentially reflecting action-dependent stabilization or synergistic control demands (Paine &

Voight, 1993; Trudeau *et al.*, 2022). At the motor unit level, both the deltoid and upper trapezius displayed higher discharge rates than the latissimus dorsi, despite no differences in normalized global RMS amplitude between them (**Figures 4c, 4d, 9**). This dichotomy between amplitude and discharge behaviour highlights the added value of motor unit analysis for interpreting muscle contributions during multi-joint shoulder actions.

Collectively, these findings highlight the limitation of relying solely on RMS amplitude from bipolar EMG, which, due to waveform cancellation or cross-talk, may not fully capture underlying neural activity (De Luca & Merletti, 1988; Day & Hulliger, 2001; Dimitrova *et al.*, 2002; Farina *et al.*, 2002, 2010; Keenan *et al.*, 2005). Therefore, the use of global EMG measures allows for a general understanding of the duration and magnitude a muscle of interest is activated, but this cannot necessarily indicate the functional role the muscle is contributing to a specific muscle action (Boettcher *et al.*, 2010). Therefore, the knowledge of motor unit behaviour during a shoulder action and the region of greatest activation may be essential to provide the information necessary to understand the functional roles of the involved muscles.

4.2 Differences within the same muscle across actions

The proposed framework allows the assessment of not only the muscles activity across actions, which we suggest is highly relevant for clinical populations, but also the assessment of the differing activation of individual muscles across actions. This type of assessment is highly relevant for basic research questions regarding the neural control of shoulder actions. To date there is a significant knowledge gap in the neural control of the shoulder, specifically concerning the deltoid and latissimus dorsi (Inglis *et al.*, 2025). As was highlighted in the systematic review and meta-analysis by Inglis, Cabral and colleagues (2025), there is much work still to be done to understand the full complexities of the shoulder. Therefore, this proposed framework would be utilized to investigate these complexities, specifically in the

618 deltoid and latissimus dorsi which both have a paucity of research, specifically involving motor
619 unit behaviour non-invasively. The precision of the proposed framework would also allow the
620 tracking of minor activation changes across shoulder angles. These activation adjustments may
621 result from trivial changes in muscle architecture (e.g. pennation angle, muscle length)
622 (Peterson & Rayan, 2011) and moment arm length (Otis *et al.*, 1994; Ackland *et al.*, 2008) that
623 have significant implications neuromechanically.

624 When examining the same muscle across different actions, clear action-dependent
625 modulation emerged at both the global and motor unit levels. The deltoid demonstrated
626 significant action-dependent modulation across the investigated shoulder actions (**Figures 4**
627 **through 9)**. Global RMS amplitude and mean motor unit discharge rate were significantly
628 greater during abduction, flexion, and extension compared to adduction, confirming its
629 multifunctional role as a primary mover across several directions (Wickham & Brown, 1998).
630 Beyond changes in activation magnitude, MUAP distribution maps for a representative
631 participant revealed a redistribution of activity across the deltoid surface (**Figures 7, 8**), with
632 anterior regions predominantly active during flexion and posterior regions during extension.
633 These findings suggest that neural control of the deltoid involves not only scaling of neural
634 drive but also selective recruitment of different motor unit populations, supporting the notion
635 of functional compartmentalization within large shoulder muscles.

636 The upper trapezius also exhibited marked action-dependent modulation. Global RMS
637 amplitude was greatest during abduction, consistent with its established role in scapular control
638 (Paine & Voight, 1993; Trudeau *et al.*, 2022). However, the spatial distribution of activation
639 varied markedly across actions, with extension eliciting a significantly higher coefficient of
640 variation compared to other actions (**Figures 4e, 4f**). At the motor unit level, discharge rates
641 were highest during abduction and lower during flexion and adduction, suggesting an action-
642 dependent adjustment of the neural drive. Together, these results demonstrate that spatial

643 distribution and motor unit variables provide complementary insights into the neural strategies
644 underlying the upper trapezius activation that are not evident from global amplitude measures
645 alone.

646 For the clavicular pectoralis major, greater global RMS amplitude and motor unit
647 discharge rates were primarily observed during flexion, whereas little activity was detected
648 during extension (**Figures 4a, 4b**). Similarly, motor units from the latissimus dorsi were
649 identified only during adduction and extension (**Table 1**). Together, these findings demonstrate
650 that muscles contributing to multiple shoulder actions are modulated not only through
651 adjustments in activation level but also through action-specific recruitment and rate coding
652 strategies.

653 Although motor units were not tracked across actions, the differences in sets of active
654 units between actions strongly suggest action- and angle-dependent recruitment and de-
655 recruitment, consistent with previous findings in other upper-limb muscles (ter Haar Romeny
656 *et al.*, 1984). These observations align with previous EMG amplitude evidence showing
657 localized activation of deltoid muscle regions dependent on action direction (Wickham &
658 Brown, 1998, 2012; Brown *et al.*, 2007), as well as similar findings in the rotator cuff muscles
659 (Alenabi *et al.*, 2018; Lulic-Kuryllo *et al.*, 2020). Importantly, the present framework extends
660 these observations by providing direct evidence at the motor unit level.

661 ***4.3 Methodological implications and future applications***

662 The capability of the proposed framework to map both spatial activation patterns
663 (**Figures 4a, 4b**) and motor unit territories and discharge patterns (**Figures 5** through **8**)
664 provides a powerful tool for probing the neural strategies underlying complex shoulder control.
665 The identification of region-specific motor unit recruitment and tonic versus phasic discharge
666 statistics offers insight into how muscles contribute to both force generation and stabilization
667 during different actions. This is evident during the extension action where the posterior deltoid

668 and upper trapezius are tonically active as they are involved in the action and the latissimus
669 dorsi is both tonically and phasically active as some motor units are recruited to support the
670 action and others (MUAPs 2-4) likely act as stabilizers (**Figure 6**). This multilevel information
671 is particularly valuable for large, multifunctional muscles such as the deltoid and upper
672 trapezius, whose roles cannot be fully understood using global EMG amplitude alone.

673 Current shoulder musculoskeletal models are based on simplified mechanical analysis
674 and often treat muscles as single force-generating elements (Hughes & An, 1997). The present
675 findings suggest that future modelling studies of the deltoid should consider within-muscle
676 heterogeneity, including compartmentalized segments (compartmentalized within segments:
677 anterior, lateral, posterior) and how this may change based on muscle architecture, moment
678 arm length and action (Hughes & An, 1997). Incorporating motor unit-level information into
679 such models may substantially improve their physiological realism and clinical relevance.

680 Finally, the differences observed between normalized RMS amplitude and motor unit
681 discharge behaviour at the group level further highlights the limitations of classic EMG-based
682 approaches. Discrepancies between global amplitude and discharge rate plausibly reflect
683 factors such as amplitude cancellation, the limited spatial coverage of HDsEMG arrays, and
684 potential cross-talk from adjacent muscles (De Luca & Merletti, 1988; Day & Hulliger, 2001;
685 Dimitrova *et al.*, 2002; Farina *et al.*, 2002; Keenan *et al.*, 2005). By directly assessing motor
686 neuron output, the proposed framework provides a more precise assessment of neural drive and
687 regional muscle involvement. This methodological advance has important implications for
688 both basic research and clinical applications, particularly in populations where subtle
689 alterations in neural control may underlie functional impairment and where targeted
690 rehabilitation strategies are required.

691 **5.0 PRACTICAL IMPLICATIONS**

- Using the proposed framework, rehabilitation programs can be designed based on the specific actions that isolate the motor unit activity, not the global muscle activity, to target specific impairments better
- The proposed framework provides a roadmap for stroke rehabilitation, where the focus may need to be centred more on motor unit recruitment and rate coding rather than on general activity within a portion of the muscle.
- The proposed framework provides a detailed description of the equipment used during the data collection including the testing jig, recording equipment, array locations and actions at each joint angle to be reproduceable for scientists and clinicians investigating recruitment of the shoulder musculature.
- The use of the robotic arm in the proposed framework allows for the testing jig and load cell to be situated so the position of the humerus, glenohumeral joint angle, muscle and moment arm length do not change across actions, only the jig moves to allow the recording of the forces produced during the specified action direction.

6.0 LIMITATIONS

Despite the rigor taken to control the specific shoulder actions and position, several limitations should be acknowledged. First, although participants were secured with straps and a rigid jig, the inherent flexibility of the shoulder complex may have introduced small variations in action execution. While this may reduce experimental control, it also increases ecological validity by better replicating strategies used in daily activities. Second, only two joint angles within the mid-range were tested, limiting extrapolation to positions closer to 0° or 180°. Third, contractions were restricted to 30% MVC, chosen to reflect moderate force demands of activities of daily living, but additional work is needed across lower and higher force levels. Fourth, the sample included only one female participant, precluding sex comparisons. Finally, only four major superficial shoulder muscles were recorded. The

inability to assess, particularly the scapular stabilizers and rotator cuff, is a key omission given their likely contribution during extension and adduction actions.

7.0 CONCLUSIONS

The present study demonstrates that it is feasible to record and analyse motor unit behaviour of major superficial shoulder muscles using HDsEMG during controlled isometric actions. The framework combines motor unit analyses with precise force measurements to provide complementary insights into neural control strategies. These methodological advances are essential for the development of comprehensive biomechanical models of the shoulder that incorporate not only anatomical and mechanical properties but also neural control strategies.

REFERENCES

Ackland DC, Pak P, Richardson M & Pandy MG (2008). Moment arms of the muscles crossing the anatomical shoulder. *Journal of Anatomy* **213,** 383–390.

Alenabi T, Whittaker R, Kim SY & Dickerson CR (2018). Maximal voluntary isometric contraction tests for normalizing electromyographic data from different regions of supraspinatus and infraspinatus muscles: Identifying reliable combinations. *Journal of Electromyography and Kinesiology* **41,** 19–26.

Baslo SA, Şirin NG, Orhan EK, Baslo MB & Öge AE (2024). Selective Muscle Involvement in Amyotrophic Lateral Sclerosis: Evidence Inferred from the Point of Motor Unit Firing Rates. *Noro Psikiyatr Ars* **61,** 296–305.

Boettcher CE, Cathers I & Ginn KA (2010). The role of shoulder muscles is task specific. *Journal of Science and Medicine in Sport* **13,** 651–656.

Brown JMM, Wickham JB, McAndrew DJ & Huang X-F (2007). Muscles within muscles: Coordination of 19 muscle segments within three shoulder muscles during isometric motor tasks. *J Electromyogr Kinesiol* **17,** 57–73.

Cabral HV, Inglis JG, Cudicio A, Cogliati M, Orizio C, Yavuz US & Negro F (2024). Muscle contractile properties directly influence shared synaptic inputs to spinal motor neurons. *The Journal of Physiology*; DOI: 10.1113/JP286078.

Chang YW, Hughes RE, Su FC, Itoi E & An KN (2000). Prediction of muscle force involved in shoulder internal rotation. *J Shoulder Elbow Surg* **9,** 188–195.

Chen M & Zhou P (2016). A Novel Framework Based on FastICA for High Density Surface EMG Decomposition. *IEEE Transactions on Neural Systems and Rehabilitation Engineering* **24,** 117–127.

Christie A, Greig Inglis J, Kamen G & Gabriel DA (2009). Relationships between surface EMG variables and motor unit firing rates. *Eur J Appl Physiol* **107,** 177–185.

Cogliati M, Cudicio A, Martinez-Valdes E, Tarperi C, Schena F, Orizio C & Negro F (2020). Half marathon induces changes in central control and peripheral properties of individual motor units in master athletes. *J Electromyogr Kinesiol* **55,** 102472.

Day SJ & Hulliger M (2001). Experimental simulation of cat electromyogram: evidence for algebraic summation of motor-unit action-potential trains. *Journal of Neurophysiology* **86,** 2144–2158.

De Luca CJ, LeFever RS, McCue MP & Xenakis AP (1982). Behaviour of human motor units in different muscles during linearly varying contractions. *The Journal of Physiology* **329,** 113–128.

De Luca CJ & Merletti R (1988). Surface myoelectric signal cross-talk among muscles of the leg. *Electroencephalography and Clinical Neurophysiology* **69,** 568–575.

Dickerson CR, Hughes RE & Chaffin DB (2008). Experimental evaluation of a computational shoulder musculoskeletal model. *Clin Biomech (Bristol)* **23,** 886–894.

Dideriksen JL, Holobar A & Falla D (2016). Preferential distribution of nociceptive input to motoneurons with muscle units in the cranial portion of the upper trapezius muscle. *Journal of Neurophysiology* **116,** 611–618.

Dimitrova NA & Dimitrov GV (2003). Interpretation of EMG changes with fatigue: facts, pitfalls, and fallacies. *J Electromyogr Kinesiol* **13,** 13–36.

Dimitrova NA, Dimitrov GV & Nikitin OA (2002). Neither high-pass filtering nor mathematical differentiation of the EMG signals can considerably reduce cross-talk. *J Electromyogr Kinesiol* **12,** 235–246.

Doherty TJ & Stashuk DW (2003). Decomposition-based quantitative electromyography: Methods and initial normative data in five muscles. *Muscle Nerve* **28,** 204–211.

Falla D & Farina D (2008*a*). Motor units in cranial and caudal regions of the upper trapezius muscle have different discharge rates during brief static contractions. *Acta Physiologica* **192,** 551–558.

Falla D & Farina D (2008*b*). Non-uniform adaptation of motor unit discharge rates during sustained static contraction of the upper trapezius muscle. *Exp Brain Res* **191,** 363–370.

Farina D, Holobar A, Merletti R & Enoka RM (2010). Decoding the neural drive to muscles from the surface electromyogram. *Clinical Neurophysiology* **121,** 1616–1623.

Farina D, Merletti R, Indino B, Nazzaro M & Pozzo M (2002). Surface EMG crosstalk between knee extensor muscles: Experimental and model results. *Muscle Nerve* **26,** 681–695.

Gerdle B, Östlund N, Grönlund C, Roeleveld K & Karlsson JS (2008). Firing rate and conduction velocity of single motor units in the trapezius muscle in fibromyalgia patients and healthy controls. *Journal of Electromyography and Kinesiology* **18,** 707–716.

ter Haar Romeny BM, van der Gon JJ & Gielen CC (1984). Relation between location of a motor unit in the human biceps brachii and its critical firing levels for different tasks. *Exp Neurol* **85,** 631–650.

Hassan A, Thompson CK, Negro F, Cummings M, Powers RK, Heckman CJ, Dewald JPA & McPherson LM (2020). Impact of parameter selection on estimates of motoneuron excitability using paired motor unit analysis. *J Neural Eng* **17,** 016063.

Hermans V, Spaepen AJ & Wouters M (1999). Relation between differences in electromyographic adaptations during static contractions and the muscle function. *Journal of Electromyography and Kinesiology* **9,** 253–261.

Holobar A, Farina D, Gazzoni M, Merletti R & Zazula D (2009). Estimating motor unit discharge patterns from high-density surface electromyogram. *Clin Neurophysiol* **120,** 551–562.

Holobar A & Zazula D (2007). Multichannel Blind Source Separation Using Convolution Kernel Compensation. *IEEE Transactions on Signal Processing* **55,** 4487–4496.

Hug F, Avrillon S, Del Vecchio A, Casolo A, Ibanez J, Nuccio S, Rossato J, Holobar A & Farina D (2021). Analysis of motor unit spike trains estimated from high-density surface electromyography is highly reliable across operators. *J Electromyogr Kinesiol*102548.

Hughes RE & An K-N (1997). Monte Carlo simulation of a planar shoulder model. *Med Biol Eng Comput* **35,** 544–548.

Hughes RE, Johnson ME, O'Driscoll SW & An K-N (1999). Age-Related Changes in Normal Isometric Shoulder Strength. *Am J Sports Med* **27,** 651–657.

Inglis JG, Cabral HV, Cosentino C, Bonardi A & Negro F (2025). Motor unit discharge behaviour in human muscles throughout force gradation: a systematic-review and meta-analysis with meta-regression. *Journal of Applied Physiology*; DOI: 10.1152/japplphysiol.00863.2024.

Joseph R, Alenabi T, Lulic T & Dickerson CR (2019). Activation of Supraspinatus and Infraspinatus Partitions and Periscapular Musculature During Rehabilitative Elastic Resistance Exercises. *American Journal of Physical Medicine & Rehabilitation* **98,** 407.

Karlsson S & Gerdle B (2001). Mean frequency and signal amplitude of the surface EMG of the quadriceps muscles increase with increasing torque — a study using the continuous wavelet transform. *Journal of Electromyography and Kinesiology* **11,** 131–140.

Keenan KG, Farina D, Maluf KS, Merletti R & Enoka RM (2005). Influence of amplitude cancellation on the simulated surface electromyogram. *Journal of Applied Physiology* **98,** 120–131.

Kelly BT, Backus SI, Warren RF & Williams RJ (2002). Electromyographic Analysis and Phase Definition of the Overhead Football Throw*. *Am J Sports Med* **30,** 837–844.

Kirk EA, Gilmore KJ, Stashuk DW, Doherty TJ & Rice CL (2019). Human motor unit characteristics of the superior trapezius muscle with age-related comparisons. *Journal of Neurophysiology* **122,** 823–832.

Kuznetsova A, Brockhoff PB & Christensen RHB (2017). lmerTest Package: Tests in Linear Mixed Effects Models. *J Stat Soft* **82,** 1–26.

Lawrence JH & De Luca CJ (1983). Myoelectric signal versus force relationship in different human muscles. *Journal of Applied Physiology* **54,** 1653–1659.

Lenth RV, Bolker B, Buerkner P, Giné-Vázquez I, Herve M, Jung M, Love J, Miguez F, Piaskowski J, Riebl H & Singmann H (2019). emmeans. Available at: https://cran.r-project.org/web/packages/emmeans/index.html [Accessed September 19, 2024].

Leonardis JM, Lulic-Kuryllo T & Lipps DB (2022). The impact of local therapies for breast cancer on shoulder muscle health and function. *Critical Reviews in Oncology/Hematology* **177,** 103759.

Lulic-Kuryllo T, Alenabi T, McDonald AC, Kim SY & Dickerson CR (2020). Sub-regional activation of supraspinatus and infraspinatus muscles during activities of daily living is task dependent. *Journal of Electromyography and Kinesiology* **54,** 102450.

Lulic-Kuryllo T, Leonardis JM, Momoh AO & Lipps DB (2023). Assessing shoulder muscle stretch reflexes following breast cancer treatment and postmastectomy breast reconstruction. *Journal of Neurophysiology*; DOI: 10.1152/jn.00081.2022.

Lulic-Kuryllo T, Negro F, Jiang N & Dickerson CR (2021*a*). Standard bipolar surface EMG estimations mischaracterize pectoralis major activity in commonly performed tasks. *Journal of Electromyography and Kinesiology* **56,** 102509.

Lulic-Kuryllo T, Negro F, Jiang N & Dickerson CR (2022). Differential regional pectoralis major activation indicates functional diversity in healthy females. *Journal of Biomechanics* **133,** 110966.

Lulic-Kuryllo T, Thompson CK, Jiang N, Negro F & Dickerson CR (2021*b*). Neural control of the healthy pectoralis major from low-to-moderate isometric contractions. *J Neurophysiol* **126,** 213–226.

Martinez-Valdes E, Negro F, Laine CM, Falla D, Mayer F & Farina D (2017). Tracking motor units longitudinally across experimental sessions with high-density surface electromyography. *J Physiol* **595,** 1479–1496.

Masuda T, Miyano H & Sadoyama T (1983). The propagation of motor unit action potential and the location of neuromuscular junction investigated by surface electrode arrays. *Electroencephalography and Clinical Neurophysiology* **55,** 594–600.

Masuda T, Miyano H & Sadoyama T (1985). A surface electrode array for detecting action potential trains of single motor units. *Electroencephalogr Clin Neurophysiol* **60,** 435–443.

Merletti R, Farina D & Granata A (1999). Non-invasive assessment of motor unit properties with linear electrode arrays. *Electroencephalogr Clin Neurophysiol Suppl* **50,** 293–300.

Negro F, Holobar A & Farina D (2009). Fluctuations in isometric muscle force can be described by one linear projection of low-frequency components of motor unit discharge rates. *The Journal of Physiology* **587,** 5925–5938.

Negro F, Muceli S, Castronovo AM, Holobar A & Farina D (2016). Multi-channel intramuscular and surface EMG decomposition by convolutive blind source separation. *J Neural Eng* **13,** 026027.

Ning Y, Zhu X, Zhu S & Zhang Y (2015). Surface EMG Decomposition Based on K-means Clustering and Convolution Kernel Compensation. *IEEE Journal of Biomedical and Health Informatics* **19,** 471–477.

Otis JC, Jiang CC, Wickiewicz TL, Peterson MG, Warren RF & Santner TJ (1994). Changes in the moment arms of the rotator cuff and deltoid muscles with abduction and rotation. *JBJS* **76,** 667.

Padovan R, Toninelli N, Longo S, Tornatore G, Esposito F, Cè E & Coratella G (2024). High-Density Electromyography Excitation in Front vs. Back Lat Pull-Down Prime Movers. *J Hum Kinet* **91,** 47–60.

Paine RM & Voight M (1993). The Role of the Scapula. *Journal of Orthopaedic & Sports Physical Therapy* **18,** 386–391.

Peterson SL & Rayan GM (2011). Shoulder and Upper Arm Muscle Architecture. *The Journal of Hand Surgery* **36,** 881–889.

Reucher H, Rau G & Silny J (1987). Spatial filtering of noninvasive multielectrode EMG: Part I--Introduction to measuring technique and applications. *IEEE Trans Biomed Eng* **34,** 98–105.

Schenkman M & Rugo de Cartaya V (1987). Kinesiology of the Shoulder Complex. *Journal of Orthopaedic & Sports Physical Therapy* **8,** 438–450.

Seth A, Dong M, Matias R & Delp S (2019). Muscle Contributions to Upper-Extremity Movement and Work From a Musculoskeletal Model of the Human Shoulder. *Front Neurorobot*; DOI: 10.3389/fnbot.2019.00090.

Stein RB, French AS, Mannard A & Yemm R (1972). New methods for analysing motor function in man and animals. *Brain Research* **40,** 187–192.

Trudeau MT, Peters JJ, Hawthorne BC, Wellington IJ, LeVasseur MR, Mancini MR, Obopilwe E, Giacomo GD, Cerciello S & Mazzocca AD (2022). The Role of the Trapezius in Stabilization of the Acromioclavicular Joint: A Biomechanical Evaluation. *Orthopaedic Journal of Sports Medicine* **10,** 23259671221118943.

Veeger HEJ & van der Helm FCT (2007). Shoulder function: The perfect compromise between mobility and stability. *Journal of Biomechanics* **40,** 2119–2129.

Westgaard RH & De Luca CJ (2001). Motor control of low-threshold motor units in the human trapezius muscle. *J Neuropathol* **85,** 1777–1781.

Wickham JB & Brown JMM (1998). Muscles within muscles: the neuromotor control of intra-muscular segments. *Eur J Appl Physiol* **78,** 219–225.

Wickham JB & Brown JMM (2012). The function of neuromuscular compartments in human shoulder muscles. *J Neurophysiol* **107,** 336–345.

Woods JJ & Bigland-Ritchie B (1983). Linear and non-linear surface EMG/force relationships in human muscles. An anatomical/functional argument for the existence of both. *Am J Phys Med* **62,** 287–299.

Yao W, Fuglevand RJ & Enoka RM (2000). Motor-Unit Synchronization Increases EMG Amplitude and Decreases Force Steadiness of Simulated Contractions. *Journal of Neurophysiology* **83,** 441–452.

AUTHOR CONTRIBUTIONS

- Conceptualization: JGI, SR, HVC, TLK, CRD, FN
- Data curation: JGI, SR, HVC
- Formal analysis: JGI, SR, HVC
- Funding acquisition: JGI, FN
- Investigation: JGI, SR, CC
- Methodology: JGI, SR, HVC, RP, TLK, CRD, FN
- Project administration: FN
- Writing – original draft: JGI, SR, HVC, FN
- Writing – review and editing: JGI, SR, HVC, CC, RP, TLK, CRD, FN